Optical and structural properties of InP quantum dots embedded in $(Al_xGa_{1-x})_{0.51}In_{0.49}P$

W.-M. Schulz,* R. Roßbach, M. Reischle, G. J. Beirne, M. Bommer, M. Jetter, and P. Michler
Institut für Halbleiteroptik und Funktionelle Grenzflächen, Universität Stuttgart, 70569 Stuttgart, Germany
(Received 20 August 2008; revised manuscript received 29 October 2008; published 30 January 2009)

Within this work we present optical and structural properties of InP quantum dots embedded in $(Al_xGa_{1-x})_{0.51}In_{0.49}P$ barriers. Atomic force microscopy measurements show a mainly bimodal height distribution with aspect ratios (ratio of width to height) of about 10:1 and quantum dot heights of around 2 nm for the smaller quantum dot class (type A) and around 4 nm for the larger quantum dot class (type B). From ensemble-photoluminescence measurements we estimated thermal activation energies of up to 270 meV for the type-A quantum dots, resulting in a 300 times higher luminescence intensity at 200 K in comparison to our InP quantum dots in $Ga_{0.51}In_{0.49}P$ at the same emission wavelength. Photon statistic measurements clearly display that InP quantum dots in $(Al_{0.20}Ga_{0.80})_{0.51}In_{0.49}P$ emit single photons up to 80 K, making them promising candidates for high-temperature single-photon emitters.

DOI: 10.1103/PhysRevB.79.035329 PACS number(s): 78.55.Et, 78.67.Hc, 42.50.Ar

I. INTRODUCTION

In contrast to existing fiber networks which use binary light pulse sequences of conventional classical light sources, several quantum cryptography protocols, such as the well-known "BB84" quantum cryptography protocol,[1] have been proposed, relying on the use of single photons as a basic structure of secure information exchange. Therefore the development and also the verification of nonclassical emitters have become very important. Many systems such as trapped single atoms, ions, and molecules have been reported to show the potential for addressing single-photon states. However, their industrial feasibility is still exiguous due to their less than ideal experimental handling, stability, and device integration. In contrast, epitaxially grown semiconductor quantum dots (QDs) provide a promising alternative due to their enormous design flexibility and *in situ* device implementation. Several approaches have been pursued, using different material systems, for example, CdSe/Zn(S,Se),[2] (In,Ga)As/GaAs,[3] GaInN/GaN,[4] and InP/(Al,Ga)InP.[5] Self-assembled InP QDs emitting within the visible red spectral range can play an important role for various novel devices. In particular because of their potential application as a nonclassical light source for the electrical generation of single photons,[6] as today Si photodetectors have their maximum photon detection efficiency in the red spectral range. A typical precondition for device applications is operation at elevated temperatures, preferably at room temperature. The band offsets in QD heterostructures have to be high enough to achieve this in a semiconductor system. In the (Al,Ga)InP material system the carrier confinement of InP QDs can be strongly increased with respect to the GaInP system by raising the aluminum content.[7] Results of structural and optical experiments of InP QDs in such $(Al_xGa_{1-x})_{0.51}In_{0.49}P$ barriers with varying aluminum content are presented in this paper, highlighting the two most promising candidates, namely, InP QDs embedded in $(Al_{0.20}Ga_{0.80})_{0.51}In_{0.49}P$ and in $(Al_{0.50}Ga_{0.50})_{0.51}In_{0.49}P$.

II. GROWTH AND EXPERIMENTAL SETUP

Our self-assembled QDs were grown by metal-organic vapor-phase epitaxy (MOVPE) with standard precursors (trimethylgallium, trimethylindium, timethylaluminum, arsine, and phosphine) at low pressure (100 mbar) on (100) GaAs substrates oriented by 6° toward the [111]*A* direction. The bottom layers consist of a 100 nm GaAs buffer layer grown at 750 °C and a 430 nm lattice-matched $(Al_xGa_{1-x})_{0.51}In_{0.49}P$ barrier ($x \in [0,1]$) grown at 720 °C, onto which the InP QDs were placed. For the standard QDs 2.1 monolayers (ML) of InP were deposited with a growth rate of 1.05 ML/s at growth temperatures between 650 and 710 °C. To examine the size-dependent characteristics of the QDs, also larger dots were fabricated by deposition of 4.2 ML InP with growth rate of 2.1 ML/s. The following 20 s growth interruption enables the QD relaxation and the ripening processes, i.e., Ostwald ripening.[8] For photoluminescence (PL) measurements, the QDs were covered with a 30 nm capping layer of $(Al_xGa_{1-x})_{0.51}In_{0.49}P$ deposited at the QD growth temperature. The capping layer was not deposited in the case of atomic force microscopy (AFM) measurements, and the samples were cooled while stabilizing with a constant phosphine gas flow.

The samples were placed in a He-flow coldfinger cryostat to enable photoluminescence measurements at variable temperatures. For the optical excitation a frequency-doubled $Ti:Al_2O_3$ laser (pulsed) for both the time-resolved and quasi-continuous-wave (cw) PLs was used. The luminescence was then dispersed by a 0.32 m Jobin Yvon monochromator system and detected using a fast multichannel plate photomultiplier tube with an effective time resolution of 30 ps.

Microphotoluminescence (μ-PL) experiments were performed with a horizontally and vertically scannable cryostat with stepper motors, providing an effective spatial resolution of 50 nm each. The light to and from the sample was guided confocally through a 50× microscope objective, focusing the laser spot down to a diameter of approximately 1 μm, using a piezoactuator. The luminescence was dispersed in this case by a 0.75 m spectrometer and detected using a liquid-nitrogen-cooled charge coupled device (CCD) camera when taking spectra (with an effective resolution of approximately 100 μeV) or two avalanche photodiodes (APDs) in a Hanbury-Brown and Twiss-type setup[9] when performing second-order autocorrelation measurements.

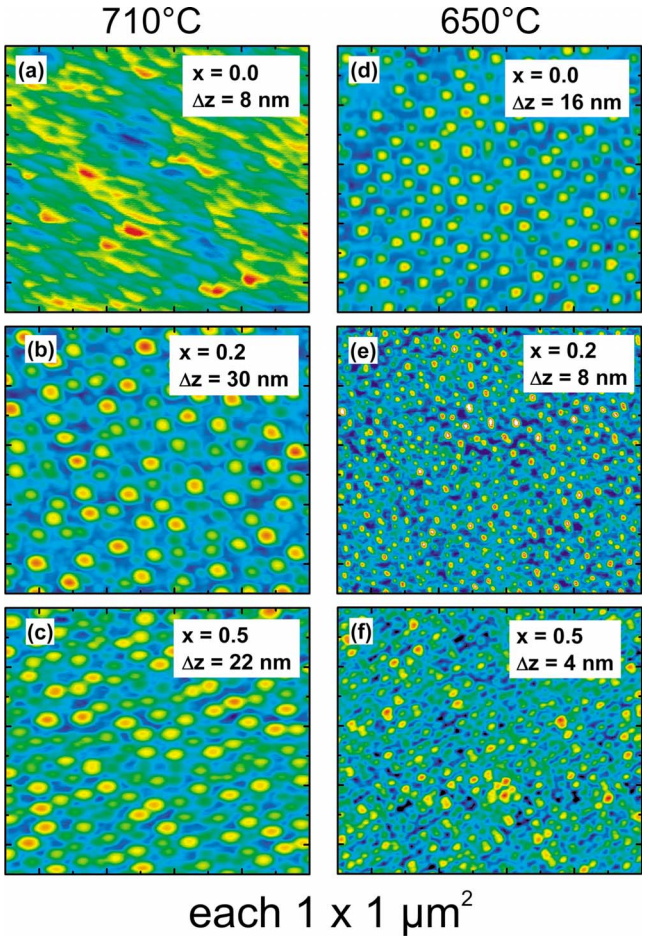

FIG. 1. (Color online) Atomic force microscope scan results from areas of 1×1 μm^2 of standard 2.1 ML uncapped InP QDs deposited [(a)–(c)] at 710 °C and [(d)–(f)] at 650 °C on different aluminum-containing $(Al_xGa_{1-x})_{0.51}In_{0.49}P$ barriers. The aluminum concentration x and the height scale Δz are given in the corresponding insets.

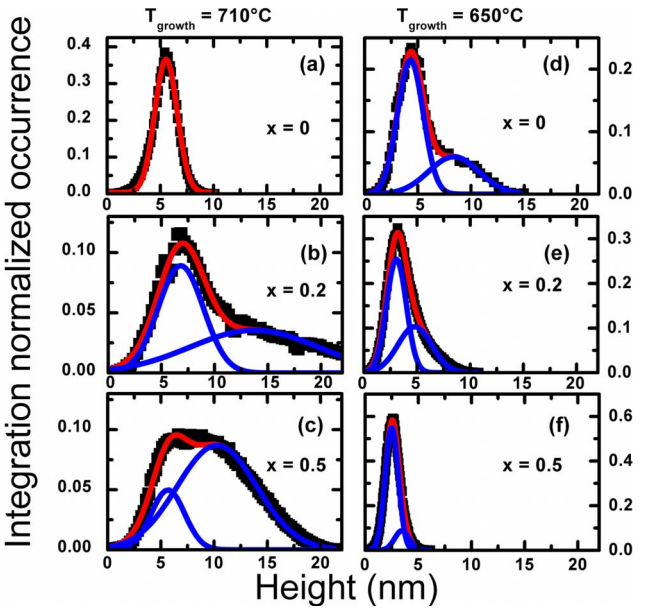

FIG. 2. (Color online) Integration-normalized height histograms of standard 2.1 ML InP QDs on $(Al_xGa_{1-x})_{0.51}In_{0.49}P$ barriers. For low aluminum contents and a growth temperature of 710 °C, the distribution is monomodal. At around $x=0.15$ the distribution gets bimodal, exhibiting a smaller QD class (type A) and a larger QD class (type B). For 650 °C deposition temperature a bimodal distribution for the whole composition range was found. The solid curves are Gaussian fits, taking into account two occurrence emphases.

III. RESULTS AND DISCUSSION

A. Structural characterization

To evaluate the structural properties of the uncapped InP QDs on different Al-containing barriers, atomic force microscopy measurements were performed using a Digital Instruments Dimension 3100 in intermittent mode. For systematic analysis, standard 2.1 ML InP QDs with barrier aluminum contents of $x=[0,0.05,0.1,0.15,0.2,0.25,0.3,0.5,0.7,1]$ manufactured at 710 °C and $x=[0,0.1,0.2,0.3,0.5,0.7,1]$ fabricated at 650 °C were investigated. Figure 1 displays the height topology of standard 2.1 ML InP QDs on $(Al_xGa_{1-x})_{0.51}In_{0.49}P$ with aluminum contents of $x=0$, $x=0.2$, and $x=0.5$ deposited [(a)–(c)] at 710 °C and at [(d)–(f)] 650 °C, respectively.

For better visibility the height scale was adapted for each image. The growth temperature and the aluminum content have a significant influence on the QD formation processes, especially regarding their size, density, and distribution. Concerning the growth temperature of 710 °C, the QD heights are below 10 nm with a relatively low density of around 1.5×10^{10} cm^{-2} for small aluminum contents ($x<0.15$). Also the QDs are slightly elongated with a noncircular shape. By incorporating more aluminum ($0.15\leq x<0.5$), the QDs grow larger in diameter and size, exceeding heights of around 20 nm. For high aluminum contents ($x\geq0.7$) the density increases as the mean base diameter gets smaller and the change in height is just minor. At growth temperature of 650 °C the situation is vice versa. For $x=0$ we measured QD heights of up to 16 nm, decreasing steadily with higher aluminum content. The QD density of this growth series is overall up to four times larger than at 710 °C deposition temperature. For a growth temperature of 710 °C we found a monomodal height distribution up to 15% Al in the barriers. At 15% Al, the distribution becomes bimodal. In contrast, at a deposition temperature of 650 °C we observed this bimodal distribution for the complete composition range under investigation. The transition from a monomodal to a bimodal height distribution with two differently sized QD types can be seen best in the height histogram.[10] The histograms in Fig. 2 illustrate statistically the measured heights and their distributions of the same structures as in Fig. 1. Only the scan area was increased to 3×3 μm^2 for statistical significance. Clearly the evolution of the smaller QD class (type A) and the formation of the larger QD class (type B) can be observed. One has to point out that at 710 °C deposition temperature the height distribution, i.e., the full width at half maximum (FWHM) of the height occurrence, is increased for aluminum-containing barriers, having a maximum at around 20% Al. For 650 °C the bimodality is reduced with increasing aluminum content. Such a bimodal height distri-

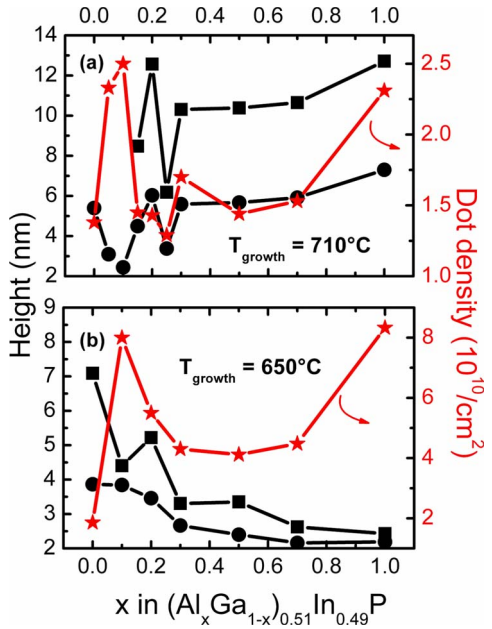

FIG. 3. (Color online) Peak heights of the smaller type-A (circles) and the larger type-B (boxes) InP QDs on $(Al_xGa_{1-x})_{0.51}In_{0.49}P$ barriers. The QDs were manufactured at (a) 710 and (b) 650 °C by depositing 2.1 ML of InP. In addition the overall QD density (stars) is provided for both growth temperatures.

bution has also been observed not only in the Ge/Si (Refs. 11 and 12) and the InAs/GaAs material systems[13,14] but also for InP QDs in GaInP.[15] This is thought to be mainly due to microscopic density fluctuations of nucleation sites, as especially in the quaternary material system, spontaneous ordering of indium- and gallium-rich layers can occur.[16]

Because there is an additional offset of around 0.5 nm arising from the misoriented wafer and the local surface condition, the fitted Gaussian occurrence maxima (solid curves) do not directly equate to the heights of the QD classes. The actual QD heights have to be evaluated separately from detailed analysis (profile measurements) of the AFM scans.

For comparison the structural parameters, the fitted peak heights of the statistical histogram evaluation, and the overall QD density (type A plus type B) of the structures are depicted in Fig. 3 for (a) 710 and (b) 650 °C. At 710 °C the QDs have a maximum height value for 20% Al in the barrier, while for 650 °C the absolute maximum height value occurs for 0% Al. Despite the nearly monotonically height decrease with higher aluminum contents, there is still a relative height maximum present for $x=0.2$ at 650 °C. Also the trends of the QD densities are comparable, although the QD density is up to four times higher for 650 °C.

To examine the structural development of the QDs, we also have doubled the deposited amount of InP at 650 °C growth temperature. Interestingly the size and the distribution are only changed slightly. For these QDs with $(Al_xGa_{1-x})_{0.51}In_{0.49}P$ barriers of $x=0.5$, we have estimated for the smaller QD class (type A) heights of approximately 2 nm and diameters of 20 nm, while the larger QD class (type B) exhibits heights of 4 nm and diameters of 40 nm. Here the average height increase only accounts for 0.5 nm for the two QD classes but changes the spectral characteristics significantly, as described in Sec. III B.

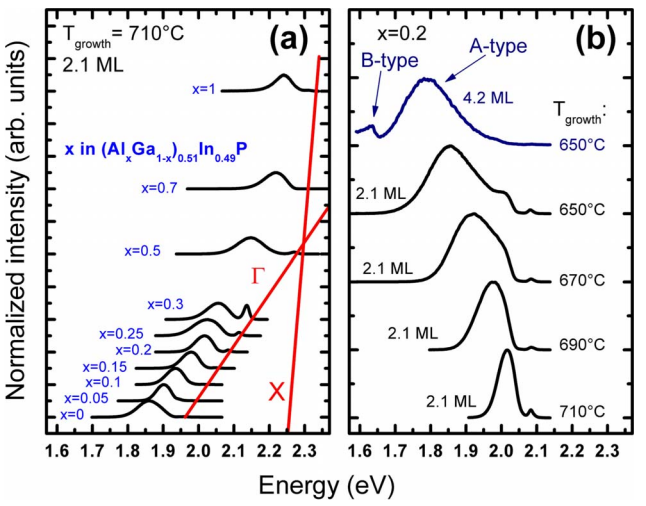

FIG. 4. (Color online) (a) Ensemble-PL spectra of standard 2.1 ML InP QDs in $(Al_xGa_{1-x})_{0.51}In_{0.49}P$ with different aluminum contents grown at 710 °C. The red lines correspond to the calculated band-gap energies of the Γ and *X* bands of the barrier. (b) Ensemble-PL spectra of standard 2.1 ML InP QDs in $(Al_{0.2}Ga_{0.8})_{0.51}In_{0.49}P$ deposited at different growth temperatures. The topmost spectrum corresponds to a deposition of 4.2 ML of InP, showing the evolution of the type-B emission.

B. Ensemble-PL

The optical properties and electronic structures of the InP QDs were examined by photoluminescence experiments. Embedding the InP QDs in Al-containing $(Al_xGa_{1-x})_{0.51}In_{0.49}P$ barriers, the barrier band-gap energy can be increased from 1.95 eV for $Ga_{0.51}In_{0.49}P$ up to 2.3 eV for $Al_{0.51}In_{0.49}P$ by raising the Al content x of the barrier from $x=0$ to $x=1$.[7] Therefore the QD confining potential can be increased in this manner.

Systematic studies were performed for QD growth temperatures between 710 and 650 °C. For this analysis, one series of standard 2.1 ML InP QDs with barrier aluminum contents as mentioned above was fabricated at 710 °C and one series with the same barrier aluminum contents was fabricated at 650 °C. Further, one series with a fixed barrier aluminum content of $x=0.2$ grown at different temperatures of $T_{Growth}=[710,690,670,650]$ °C was investigated. For comparison, two structures with 4.2 ML of InP and barrier aluminum contents of $x=0.2$ and $x=0.5$ were deposited at 650 °C.

Initially, cw PL measurements were performed to investigate the emission energy of the QD ensemble with respect to the Al content of the $(Al_xGa_{1-x})_{0.51}In_{0.49}P$ barrier. Figure 4(a) displays the spectra for 2.1 ML InP grown at 710 °C at a measurement temperature of 5 K and excitation power density of 700 W cm^{-2} at which state filling does not occur yet. The maximum of the QD PL intensity shifts with increasing barrier Al content from 1.85 eV for $x=0$ to 2.24 eV for $x=1$.[17] The QD energy rises with increasing barrier energy due to increasing Al content. This is mainly because of additional incorporation of Al and Ga out of the barrier into the QDs during their growth. The peak corresponding to the barrier follows nearly perfectly the theoretically calculated

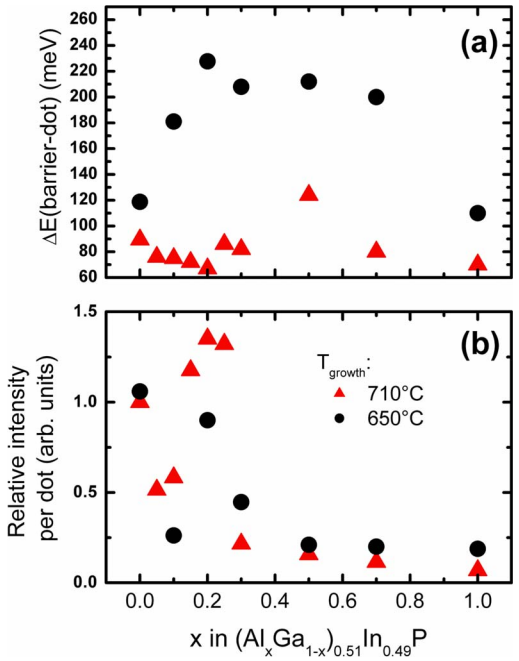

FIG. 5. (Color online) (a) Confinement energies and (b) relative PL intensities per dot of standard 2.1 ML InP QDs in $(Al_xGa_{1-x})_{0.51}In_{0.49}P$ with different aluminum contents grown at 710 °C (triangles) and at 650 °C (boxes). The relative intensities per dot of the structures were scaled with respect to the normalized intensity per dot of the InP QDs in $Ga_{0.51}In_{0.49}P$ grown at 710 °C.

band-gap energy of the $(Al_xGa_{1-x})_{0.51}In_{0.49}P$ bulk barrier [straight lines in Fig. 4(a)].[7] Due to the Al and Ga incorporation the confinement energy ΔE, which is the energy difference between the QD ensemble and the barrier emission, remains relatively small for all the structures. To increase ΔE, the suppression of incorporation of the barrier atoms was tried by reducing the growth temperature successively down to a value of 650 °C. This leads to a decrease in the diffusion length of the migrating atoms, resulting in QDs emitting at lower emission energies, as shown in Fig. 4(b) for standard 2.1 ML InP QDs in $(Al_{0.20}Ga_{0.80})_{0.51}In_{49}P$ and a confinement energy ΔE of around 230 meV. The high-energy shoulder of the structure grown at 650 °C emitting at around 2 eV can be attributed to the wetting layer as the low growth temperature conveys two-dimensional growth.

Over the complete composition range we observed a nonlinear dependence of the luminescence intensity of the QDs on the confinement energy ΔE. Figure 5(a) depicts the confinement energies of the QDs grown at 710 °C (triangles) and at 650 °C (circles). For the high growth temperature the confinement energy has a value of 90 meV for $Ga_{0.51}In_{0.49}P$ barriers, decreases to 65 meV for $(Al_xGa_{1-x})_{0.51}In_{0.49}P$ barriers with $x=0.2$, and shows an absolute maximum of 120 meV for 50% Al in the barrier. At low growth temperature ΔE can be increased linearly up to 230 meV for $(Al_{0.2}Ga_{0.8})_{0.51}In_{0.49}P$ and decreases to 110 meV for $Al_{0.51}In_{0.49}P$. Although the low growth temperature reduces the QDs' heights and increases the quantum size effect, the confinement energy can be strongly enhanced with respect to the high growth temperatures. Therefore we conclude that the Al and Ga incorporation can be violently suppressed in this manner.

In addition, by varying the Al content of the barrier, the QD density slightly changes even for constant growth temperatures. To compare the luminescence behaviors of the different structures, we calculated therefore the ratio of the relative luminescence intensities and the QD densities for each sample (the densities were deduced from AFM measurements). The results are displayed in Fig. 5(b). The evaluated luminescence yield per QD emitter reaches a (relative) maximum for 20% Al in the barrier and strongly decreases for higher Al contents. The generation of nonradiative recombination centers through the contamination of Al with residual oxygen and the effects of approaching the crossover point between the Γ band and X band are thought to cause this decrease.[18,19] For the low growth temperature the QDs with $Ga_{0.51}In_{0.49}P$ barriers show the highest emitter intensity. But in comparison to the QDs with 20% Al in the barrier, they exhibit a much smaller confinement energy, which causes a strong decrease in the PL intensity specially at elevated temperatures, as discussed later on.

A further increase in the carrier confinement, resulting in an enhancement of the PL intensity at elevated temperatures, can be achieved by deposition of larger QDs to reduce the quantum size effect.[20] For this purpose we deposited a larger amount of InP, 4.2 ML instead of 2.1 ML, for the QD growth at 650 °C on $(Al_{0.20}Ga_{0.80})_{0.51}In_{0.49}P$ and $(Al_{0.5}Ga_{0.5})_{0.51}In_{0.49}P$, respectively. For barriers with an aluminum content of 20% a total confinement energy of $\Delta E = 270$ meV could be achieved, as displayed in the topmost spectra of Fig. 4(b). By applying this growth scenario, a slightly enhanced bimodal distribution was found in AFM measurements (not shown here). The larger amount of deposited InP leads on one hand to the formation of larger QDs due to the presence of a multitude of nucleation sites especially in the high-aluminum-content barrier and the reduced surface mobility at the lower growth temperatures. On the other hand, a fraction of the smaller QD sizes are still present as they do not ripen to larger ones. This enhanced bimodal distribution is also visible in the luminescence spectrum of the sample where the emission of the type-B QDs is visible at around 1.63 eV. Emission from type-B QDs at approximately 1.63 eV was also reported for the InP/(Al,Ga)InP material system by other groups.[21,22] The spectral bimodality is even more pronounced for the structure with 50% Al in the barrier. Figure 6 shows the corresponding temperature-dependent spectra of the 4.2 ML InP QDs in $(Al_{0.5}Ga_{0.5})_{0.51}In_{0.49}P$, excited with power density of 700 W cm^{-2} at which state filling was not yet observable.

One can clearly see the GaAs luminescence at around 1.5 eV and the $(Al_{0.5}Ga_{0.5})_{0.51}In_{0.49}P$ barrier emitting at 2.3 eV. The resonance peak at 1.62 eV corresponds to the larger type-B QDs, the peak at 1.92 eV corresponds to the smaller type-A QDs, and the low-intensity shoulder at 2.17 eV could be attributed to the wetting layer. The total confinement ΔE of 350 meV for type A and 630 meV for type B (251 meV for type A and 549 meV for type B when considering the energetic difference between QDs and wetting layer) can be deduced from Fig. 6. The barrier luminescence completely vanishes for temperatures above 100 K due to nonradiative loss mechanisms.

The temperature-dependent intensity behavior can be described well by applying a simple thermal activation

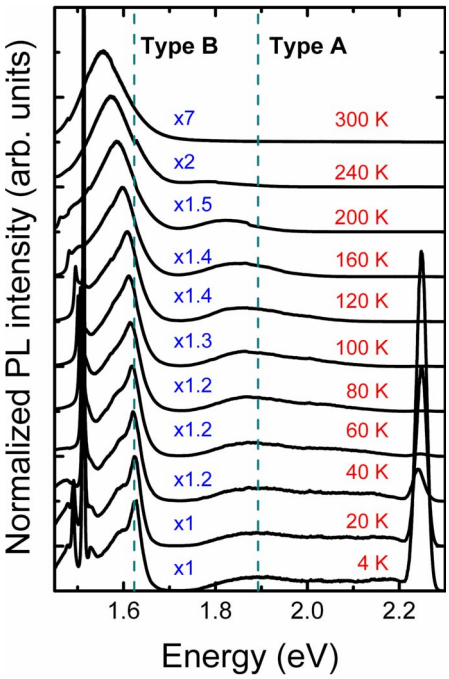

FIG. 6. (Color online) Temperature-dependent ensemble-PL spectra of 4.2 ML InP QDs in $(Al_{0.5}Ga_{0.5})_{0.51}In_{0.49}P$ grown at 650 °C. The dashed vertical lines are guides for the eyes and indicate the emission features from the two QD classes. At elevated temperatures the larger, lower-energy type-B QDs dominate the luminescence spectra.

model.[23,24] As the temperature dependence could not be fitted adequately with only one activation energy, for each QD class we took two activation energies E_1^A and E_2^A, and E_1^B and E_2^B for both type-A and type-B QDs into account:

$$I_A(T) = \frac{a_1 I_A}{1 + a_1 e^{E_1^A/k_B T}} + \frac{a_2 I_A}{1 + a_2 e^{E_2^A/k_B T}}, \quad (1)$$

$$I_B(T) = \frac{b_1 I_B}{1 + b_1 e^{E_1^A/k_B T}} + \frac{b_2 I_B}{1 + b_2 e^{E_2^A/k_B T}}, \quad (2)$$

where $I_{A,B}$ is the initial integrated PL intensity of the two QD classes at the lowest temperature ($T=5$ K), $a_{1,2}$ and $b_{1,2}$ are temperature-independent constants, and k_B is the Boltzmann constant. Therefore, by fitting the luminescence intensity behaviors for both type-A and type-B QDs separately (see inset of Fig. 7), the intensity ratio $R(T)$ of the luminescence intensities of the two QD types can be written as the ratio of Eq. (1) to Eq. (2):

$$R(T) = \frac{I_A(T)}{I_B(T)}. \quad (3)$$

This experimental intensity ratio is displayed in Fig. 7.

The ratio $R(T)$ remains more or less constant for low temperatures but changes abruptly at around 100 K. At 120 K it reaches its maximum value, and then decreases continuously for higher temperatures. This behavior may be explained based on the structural differences between the two QD classes, especially their size. Due to the reduced quantization, the larger type-B QDs have a smaller energy-level spacing and therefore more energy levels in the QD than the type-A QDs. Although the density of the type-B QDs is much lower than the density of the type-A QDs, the integrated low-temperature luminescence intensity of the type-B QDs is higher than the luminescence intensity of the type-A QDs. The carrier capture and relaxation processes are more efficient for the larger type-B QDs due to their smaller energy-level spacing.[25] In addition the high number of available energy levels in the type-B QDs may lead to a higher population number of carriers in the QDs. This can result in a more intense luminescence intensity.[26]

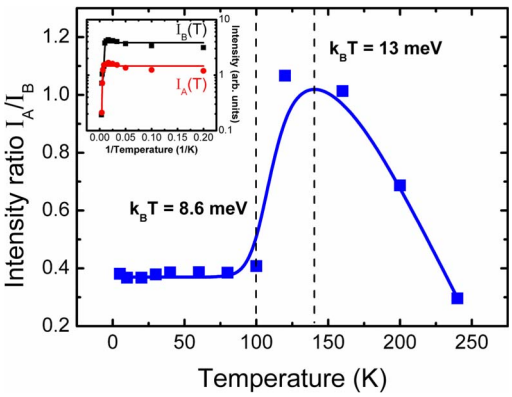

FIG. 7. (Color online) Temperature-dependent ratio of the integrated intensity of the two dot classes type A and type B (see Fig. 6). The solid curve is the fit using the model, while the inset shows the integrated PL intensity of both QD types and the corresponding Arrhenius fits which were applied separately. The two dashed vertical lines indicate the temperatures at which key changes in intensity ratio occur. The associated thermal energies k_BT are also displayed.

In particular for high temperature the type-B QDs dominate the spectra, even at elevated temperatures up to room temperature. In fact, the carrier redistribution over density of states favors the emission on the low-energy side of the QDs band.

A complete similar temperature dependence of the intensity ratio was observed for the structure with 4.2 ML InP in $(Al_{0.2}Ga_{0.8})_{0.51}In_{0.49}P$ fabricated at 650 °C [see Fig. 4(b)]. But as the bimodality is not as pronounced as in the case for $x=0.5$, the step of the intensity ratio with temperature is smaller and therefore is not shown here.

By fitting the experimental data according to this model, we deduced activation energies of $E_1^A=269$ meV and $E_2^A=219$ meV for the type-A QDs and $E_1^B=271$ meV and $E_2^B=85$ meV for the type-B QDs. The estimated energy of E_1^A corresponds well to the total localization depth of the type-A QDs with respect to the wetting layer, while E_1^B corresponds to approximately half of the localization depth of the type-B QDs with respect to the wetting layer. This behavior indicates the uncorrelated loss of holes or electrons for type-A QDs, while for type-B QDs the whole exciton seems to be thermally activated out of the QDs.[27] For the structure with 4.2 ML InP in $(Al_{0.2}Ga_{0.8})_{0.51}In_{0.49}P$ fabricated at 650 °C, the activation energies are smaller due to the reduced total confinement energy, but indicate the same activation processes

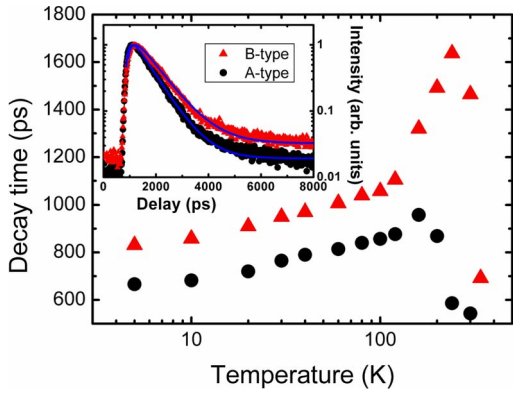

FIG. 8. (Color online) Temperature-dependent decay times obtained from type-A QDs (circles) and type-B QDs (triangles) of Fig. 6. The inset shows the monoexponential transients with their corresponding fits (solid curves) according to Ref. 30. For elevated temperatures the decay times decrease strongly due to additionally activated nonradiative decay channels.

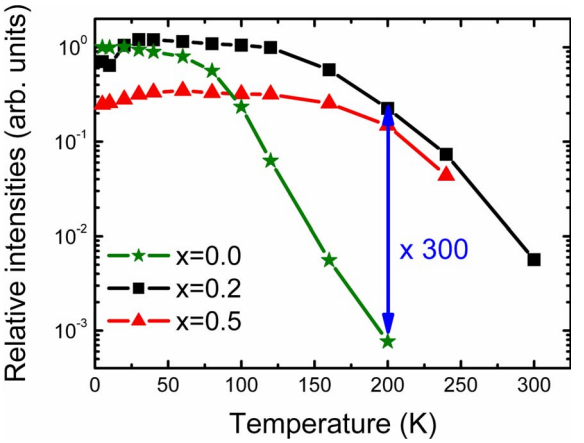

FIG. 9. (Color online) Relative PL intensities of type-A QDs of standard 2.1 ML InP in $Ga_{0.51}In_{0.49}P$ deposited at 710 °C (stars) and 4.2 ML InP in $(Al_{0.2}Ga_{0.8})_{0.51}In_{0.49}P$ (boxes) and in $(Al_{0.5}Ga_{0.5})_{0.51}In_{0.49}P$ (triangles) both grown at 650 °C. The intensities are normalized with respect to the low-temperature intensity (5 K) of the InP/GaInP QDs.

(E_1^A=240 meV, E_2^A=28 meV, E_1^B=230 meV, and E_2^B=89 meV). The quenching state could be the wetting layer, through which the thermally excited carriers can reach nonradiative recombination centers at the heterostructure interface or in the barrier.[28] Subsequent transport in the wetting layer and recapture processes of the carriers can occur alternatively.[29] Such enhanced nonradiative decay rates can give rise to strongly decreasing decay times. In Fig. 8 the temperature-dependent experimental decay times obtained from time-resolved PL measurements are depicted. As an example, in the inset of Fig. 8 the time transients of the corresponding PL maximum at 5 K can be seen for the type-A QDs (circles) and the type-B QDs (triangles). The transients exhibit one fast (delay range of 1–4 ns) and one slow (delay range of 4–8 ns) decay channel. Up to a delay of 4 ns the transients can be described very accurately with only one (fast) decay component. The fitting error for the slow decay component would be very large due to the low luminescence intensity for large delays. Because of this we used a model of the random initial occupation[30] comprising one decay channel to determine the fast decay times. The QDs display an approximately constant decay time for low temperatures with a linear increase at higher temperatures.[31] Above a certain critical temperature the decay times decrease violently. This decrease seen at high temperatures and the fact that the drop temperature is even higher for the larger type-B QDs suggest that the temperature-dependent PL decay indeed is a consequence of additional nonradiative decay channels. Very similar results were reported for InAs/GaAs QDs in Ref. 32. The higher decay time of approximately 830 ps (5 K) observed for the larger type-B QDs when compared to approximately 670 ps for the type-A QDs is thought to be due to the reduced wave-function overlap integral. We therefore think that the nonexpected intensity ratio in Fig. 7 is on the basis of the very different drop temperatures, namely, 160 K for type A and 240 K for type B, in addition to the different thermal activation energies. A complete similar temperature dependence of the decay times was observed for the structure with 4.2 ML InP in $(Al_{0.2}Ga_{0.8})_{0.51}In_{0.49}P$ fabricated at 650 °C. Decay times of 572 ps for type-A QDs and 785 ps for type-B QDs at 5 K were observed, while the drop temperatures were estimated to be 160 K for type-A QDs and about 200 K for type-B QDs.

The temperature behavior of the PL intensity of the 4.2 ML InP QDs in $(Al_{0.2,0.5}Ga_{0.8,0.5})_{0.51}In_{0.49}P$ grown at 650 °C with respect to 2.1 ML InP QDs in $Ga_{0.51}In_{0.49}P$ grown at 710 °C can be best shown by comparing their relative intensities as shown in Fig. 9 for the type-A QDs. One has to point out that the type-A QDs of these three structures exhibit approximately the same wavelength, which could be very important for future device applications due to detector characteristics. For this the relative intensities were normalized with respect to their initial intensity at 5 K of $InP/Ga_{0.51}In_{0.49}P$ QDs. The luminescence intensity for $InP/Ga_{0.51}In_{0.49}P$ QDs (stars) decreases continuously from 5 K onward. The InP QDs in aluminum containing barriers show a significant increase in their intensities up to 40 K, which is due to thermal activation of carriers trapped at low temperatures in shallow localization centers of the quaternary barrier. These band-edge states are formed because of microscopic compositional fluctuations in the $(Al_xGa_{1-x})_{0.51}In_{0.49}P$ barriers. For low-aluminum-content barriers the absolute intensities are about five times higher than for the higher-aluminum-content $InP/(Al_{0.50}Ga_{0.50})_{0.51}In_{0.49}P$ QDs. Although the $InP/(Al_{0.5}Ga_{0.5})_{0.51}In_{0.49}P$ QDs have the highest confinement energy, the intensity of the $InP/(Al_{0.2}Ga_{0.8})_{0.51}In_{0.49}P$ QDs is much higher, even at elevated temperatures. At 150 K the QDs in these barriers still possess the same intensity as at 5 K. Therefore, when compared with $InP/Ga_{0.51}In_{0.49}P$ QDs at 200 K, the relative intensity for the $InP/(Al_{0.2}Ga_{0.8})_{0.51}In_{0.49}P$ QDs is 300 times higher.

C. Microphotoluminescence

To confirm the zero-dimensionality of the QDs, μ-PL and second-order autocorrelation measurements were performed

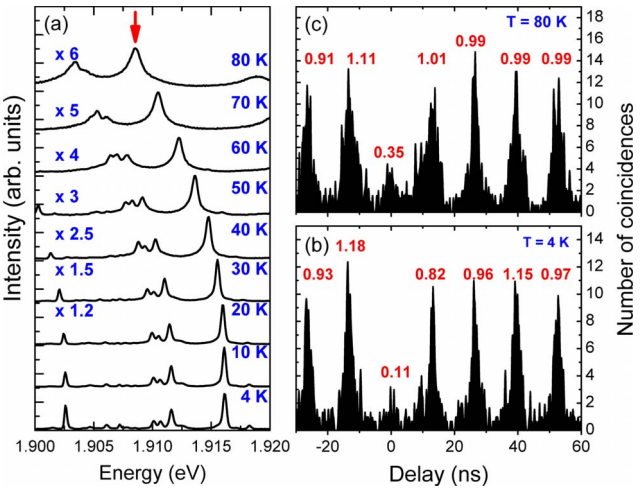

FIG. 10. (Color online) (a) Temperature-dependent single-QD μ-PL measurements and second-order autocorrelation measurements performed (b) at 4 K and (c) at 80 K. The autocorrelation measurements were performed on the emission line indicated by the (red) arrow. Growth conditions: 4.2 ML of InP deposited at 650 °C.

on the samples described earlier. To select single QDs out of the ensemble, the samples were covered with a shadow mask of 50-nm-thick chromium with aperture diameter of 750 nm using a microsphere process.[33] Figure 10(a) displays characteristic μ-PL spectra of a single QD embedded in an $(Al_{0.2}Ga_{0.8})_{0.51}In_{0.49}P$ barrier that emits at 1.916 eV at 4 K (equivalent height was 4.2 ML InP deposited at 650 °C). The other peaks result from several other QDs that are excited within the same aperture. The relatively large linewidth of 317 μeV at 4 K is due to local carrier density fluctuations around the QD, an effect that is also known as spectral diffusion,[34] and is therefore not equal to the homogeneous linewidth. The influence of spectral diffusion is even more pronounced for larger nanostructures, which currently limited our single-emitter measurements to the smaller type-A QDs. The larger type-B QDs were not individually resolvable with our aperture diameter. On this intense single-QD peak we performed pulsed second-order autocorrelation measurements $[g^{(2)}(\tau)]$ at different temperatures, shown in Fig. 10 for (b) 4 and (c) 80 K. The area of the coincidence peak at $\tau=0$ is equivalent to (b) 11% and (c) 35% of the Poisson-normalized level, which was calculated from the averaged coincidence data. Therefore, when compared to a Poissonian light source of the same average intensity, multiphoton emission pulses (bunching) were suppressed by a factor of 9 (4 K) and a factor of 3 (80 K).

In order to obtain information about the phonon coupling, the peak position of the single QD is plotted in Fig. 11(a). The temperature dependence of the exciton transition energy, which decreases from 1.916 eV at 5 K to 1.909 eV at 80 K, can be well described using the following equation:[35]

$$E_X(T) = E_X(0) - S\langle E_{\rm ph}\rangle[\coth(\langle E_{\rm ph}\rangle/2k_BT) - 1], \qquad (4)$$

where $E_X(0)$ is the excitonic transition energy at 0 K, S is a dimensionless coupling constant, and $\langle E_{\rm ph}\rangle$ is an average phonon energy which corresponds to the phonon-carrier coupling. By performing this fit to the data an average phonon energy of $\langle E_{\rm ph}\rangle = 11.1$ meV could be evaluated for the $InP/(Al_{0.2}Ga_{0.8})_{0.51}In_{0.49}P$ QDs. This energy seems to correspond to the transverse-acoustic phonon of $\langle E_{\rm ph}\rangle = 11.2$ meV of $Ga_{0.51}In_{0.49}P$ (Refs. 36 and 37) for low-Al-content barriers.[38] Furthermore, the linewidth (full width at half maximum of the exciton peak) increases from 317 μeV at 5 K to 1090 μeV at 80 K. The change in linewidth with temperature can be described by the following relation:[39,40]

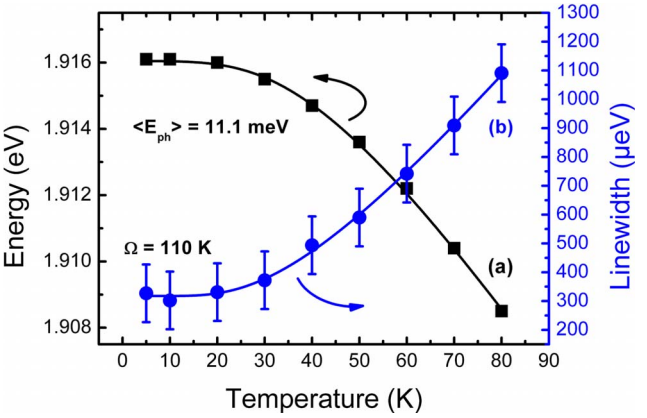

FIG. 11. (Color online) Temperature-dependent (a) excitonic transition energies and (b) FWHMs corresponding to the QD in Fig. 10. The solid curves are fits according to the models described in Eqs. (4) and (5) (Refs. 35, 39, and 40).

$$\Gamma(T) = \Gamma(0) + \Gamma_f \frac{1}{e^{\Omega/T} - 1}, \qquad (5)$$

where $\Gamma(0)$ represents the broadening due to the temperature-independent broadening mechanisms, and Γ_f is the strength of the exciton-phonon coupling. This semiempirical formula comprises an average Bose-Einstein statistical factor with Ω as the effective temperature needed for phononic excitation. The fit results in an effective temperature of $\Omega = (110 \pm 10)$ K, which corresponds to a thermal energy of $k_BT \approx (10 \pm 1.5)$ meV. This value is slightly below the average phonon energy $\langle E_{\rm ph}\rangle$ of 11.2 meV. Although this is not a definite proof of this model, we conclude that the exciton interaction with low-frequency acoustic phonons is consistent with the observed linewidth temperature evolution. Therefore, we propose that the temperature-dependent redshift and linewidth broadening are both associated with the same phonon.

The same μ-PL experiments were performed using the structure with 50% Al (4.2 ML, 650 °C). Due to high uncorrelated background, which probably arises from an increased trap density within the high-aluminum-content barriers and the five times lower intensity, the measurements are currently restricted to low temperatures. Here, the measured linewidth of 352 μeV also indicates strong effects of spectral diffusion.

IV. CONCLUSION

We have presented structural and optical properties of InP quantum dots in different $(Al_xGa_{1-x})_{0.51}In_{0.49}P$ barriers. We

have observed a mainly bimodal size distribution with a smaller (type-A) and a larger (type-B) QD class that also can be visible in ensemble-PL for high growth rates. For growth temperature of 710 °C a strong incorporation of Al and Ga into the QDs occurs. By reducing the deposition temperature down to 650 °C, the confinement energies can be enhanced with higher aluminum contents of the barrier. Therefore high confinement energies of up to 270 meV for the smaller type-A class of 4.2 ML InP QDs in $(Al_{0.2}Ga_{0.8})_{0.51}In_{0.49}P$ could be achieved, showing a residual luminescence intensity of 60% at 200 K when compared to their luminescence intensity at 5 K. The PL intensity of the QD emission has a maximum for the $(Al_{0.2}Ga_{0.8})_{0.51}In_{0.49}P$ barrier and is about 300 times larger than that of the InP QDs in $Ga_{0.51}In_{0.49}P$ at 200 K. It was therefore possible to record single-photon emission characteristics of a QD up to 80 K. This demonstrates that it is possible to achieve single-photon emission in the red spectral range with only liquid-nitrogen cooling.

ACKNOWLEDGMENTS

The authors would like to thank E. Kohler for technical assistance with the MOVPE system, and H. Graebeldinger and M. Ubl for doing the device processing. They acknowledge the partial financial support for this work that was granted by the Deutsche Forschungsgemeinschaft Forschergruppe FOR 730 and the SFB TRR 21.

*Corresponding author. FAX: +49-711-685-63866. m.schulz@ihfg.uni-stuttgart.de

[1] C. H. Bennett and G. Brassard, Proceedings of IEEE International Conference on Computers, Systems and Signal Processing, Bangalore, India, 1984 (unpublished), Vol. 11, p. 175.
[2] K. Sebald, P. Michler, T. Passow, D. Hommel, G. Bacher, and A. Forchel, Appl. Phys. Lett. **81**, 2920 (2002).
[3] P. Michler, A. Kiraz, C. Becher, W. V. Schoenfeld, P. M. Petroff, L. Zhang, E. Hu, and A. Imamoglu, Science **290**, 2282 (2000).
[4] S. Kako, C. Santori, K. Hoshino, S. Goetzinger, Y. Yamamoto, and Y. Arakawa, Nature Mater. **5**, 887 (2006).
[5] V. Zwiller, T. Aichele, W. Seifert, J. Persson, and O. Benson, Appl. Phys. Lett. **82**, 1509 (2003).
[6] M. Reischle, G. J. Beirne, W.-M. Schulz, M. Eichfelder, R. Roßbach, M. Jetter, and P. Michler, Opt. Express **16**, 12771 (2008).
[7] L. Börnstein, *Numerical Data and Functional Relationship in Science and Technology*, 17th ed., edited by K.-H. Hellwege and O. Madelung (Springer, New York, 1982).
[8] J. Lyklema, *Fundamentals of Interface and Colloid Science I: Fundamentals* (Academic, San Diego, 1991).
[9] R. Hanbury-Brown and R. Q. Twiss, *The Physics of Quantum Information Technology* (Springer, Berlin, 2000).
[10] J. Porsche, A. Ruf, M. Geiger, and F. Scholz, J. Cryst. Growth **195**, 591 (1998).
[11] D. J. Eaglesham and M. Cerullo, Phys. Rev. Lett. **64**, 1943 (1990).
[12] M. Tomitori, K. Watanabe, M. Kobayashi, and O. Nishikawa, Appl. Surf. Sci. **76-77**, 322 (1994).
[13] H. Saito, K. Nishi, I. Ogura, S. Sugou, and Y. Sugimoto, Appl. Phys. Lett. **69**, 3140 (1996).
[14] H. Kissel, U. Muller, C. Walther, W. T. Masselink, Y. I. Mazur, G. G. Tarasov, and M. P. Lisitsa, Phys. Rev. B **62**, 7213 (2000).
[15] G. J. Beirne, M. Jetter, H. Schweizer, and P. Michler, J. Appl. Phys. **98**, 093522 (2005).
[16] A. Gomyo, S. Kawata, T. Suzuki, S. Iijima, and I. Hino, Jpn. J. Appl. Phys., Part 2 **28**, L1728 (1989).
[17] R. Roßbach, W.-M. Schulz, M. Reischle, G. J. Beirne, M. Jetter, and P. Michler, J. Cryst. Growth **298**, 595 (2007).
[18] D. S. Cao, A. W. Kimball, and G. B. Stringfellow, J. Appl. Phys. **67**, 739 (1990).
[19] S. Naritsuka, Y. Nishikawa, H. Sugawara, M. Ishikawa, and Y. Kokubun, J. Electron. Mater. **20**, 687 (1991).
[20] A. Kurtenbach, K. Eberl, and T. Shitara, Appl. Phys. Lett. **66**, 361 (1995).
[21] J. Porsche, M. Ost, F. Scholz, A. Fantini, F. Phillipp, T. Riedl, and A. Hangleiter, IEEE J. Sel. Top. Quantum Electron. **6**, 482 (2000).
[22] P. M. Smowton, J. Lutti, G. M. Lewis, A. B. Krysa, J. S. Roberts, and P. A. Houston, IEEE J. Sel. Top. Quantum Electron. **11**, 1035 (2005).
[23] M. Sugisaki, Hong-Wen Ren, K. Nishi, and Y. Masumoto, Jpn. J. Appl. Phys., Part 1 **41**, 958 (2002).
[24] M. Grundmann, R. Heitz, N. Ledentsov, O. Stier, D. Bimberg, V. M. Ustinov, P. S. Kopév, Zh. I. Alferov, S. S. Ruvimov, P. Werner, U. Gösele, and J. Heydenreich, Superlattices Microstruct. **19**, 81 (1996).
[25] S. Grosse, J. H. H. Sandmann, G. von Plessen, J. Feldmann, H. Lipsanen, M. Sopanen, J. Tulkki, and J. Ahopelto, Phys. Rev. B **55**, 4473 (1997).
[26] C. M. A. Kapteyn, M. Lion, R. Heitz, and D. Bimberg, Appl. Phys. Lett. **76**, 1573 (2000).
[27] P. Michler, A. Hangleiter, M. Moser, M. Geiger, and F. Scholz, Phys. Rev. B **46**, 7280 (1992).
[28] T. B. Norris, K. Kim, J. Urayama, Z. K. Wu, J. Singh, and P. K. Bhattacharya, J. Phys. D **38**, 2077 (2005).
[29] S. Sanguinetti, M. Henini, M. Grassi Alessi, M. Capizzi, P. Frigeri, and S. Franchi, Phys. Rev. B **60**, 8276 (1999).
[30] K. Mukai and M. Sugawara, *Semiconductors and Semimetals* (Academic, New York, 1999), Vol. 60, p. 209.
[31] D. S. Citrin, Superlattices Microstruct. **13**, 303 (1993).
[32] W. Yang, R. R. Lowe-Webb, H. Lee, and P. C. Sercel, Phys. Rev. B **56**, 13314 (1997).
[33] U. Håkanson, J. Persson, F. Persson, H. Svensson, L. Montelius, and M. K. J. Johansson, Nanotechnology **14**, 675 (2003).
[34] F. Wang, A. Badolato, I. Wilson-Rae, P. M. Petroff, E. Hu, J. Urayama, and A. Imamoglu, Appl. Phys. Lett. **85**, 3423 (2004).
[35] K. P. O'Donnell and X. Chen, Appl. Phys. Lett. **58**, 2924 (1991).
[36] G. F. Alfrey and P. H. Borcherds, J. Phys. C **5**, L275 (1972).
[37] P. Merle, D. Auvergne, H. Mathieu, and J. Chevallier, Phys. Rev. B **15**, 2032 (1977).
[38] T. Hofmann, G. Leibiger, V. Gottschalch, I. Pietzonka, and M. Schubert, Phys. Rev. B **64**, 155206 (2001).
[39] P. Lautenschlager, M. Garriga, L. Vina, and M. Cardona, Phys. Rev. B **36**, 4821 (1987).
[40] L. Viña, S. Logothetidis, and M. Cardona, Phys. Rev. B **30**, 1979 (1984).